10-14-2009

Infrasonic Ambient Noise Interferometry From Correlations of Microbaroms

Matthew M. Haney
Boise State University

 DOI: 10.1029/2009GL040179

Infrasonic ambient noise interferometry from correlations of microbaroms

M. M. Haney[1,2]

Received 21 July 2009; revised 28 August 2009; accepted 10 September 2009; published 14 October 2009.

[1] We show that microbaroms, continuous infrasound fluctuations resulting from the interaction of the ocean with the atmosphere, have long-range correlation properties that make it possible to estimate the impulse response between two microphones from passive recordings. The processing is analogous to methods employed in the emerging field of ambient noise seismology, where the random noise source is the ocean coupling with the solid Earth (microseisms) instead of the atmosphere (microbaroms). We find that time-dependent temperature fields and temperature inversions determine the character of infrasonic impulse responses at Fourpeaked Volcano in Alaska. Applications include imaging and monitoring the gross structure of the Earth's atmospheric boundary layer. **Citation:** Haney, M. M. (2009), Infrasonic ambient noise interferometry from correlations of microbaroms, *Geophys. Res. Lett.*, *36*, L19808, doi:10.1029/2009GL040179.

1. Introduction

[2] The acoustic structure of the atmosphere determines the distribution of infrasonic waveguides and shadow zones and bears the imprint of heterogeneous temperature and wind fields [*Ostashev et al.*, 2005]. Knowing atmospheric acoustic structure is thus critical for determining the transmission quality of infrasonic sources, either natural (e.g., volcanic) or man-made. Besides analysis of infrasonic sources, the sensitivity of sound to temperature and wind fields offers a way to study important meteorological phenomena, such as the atmospheric boundary layer and turbulence. For instance, acoustic tomography has been proposed to map atmospheric structure with a network of high-frequency sources and receivers [*Wilson and Thomson*, 1994]. Man-made infrasonic sources with frequencies below 20 Hz, however, can be difficult to implement. Responding to this issue, *Bedard and Georges* [2000] have stated that to study the propagation of infrasound "it would be useful to be able to generate coherent narrowband infrasound at will." Infrasound is particularly useful since it is able to propagate over thousands of kilometers in the atmosphere [*Bedard and Georges*, 2000].

[3] Recently it has been demonstrated that cross-correlations of passive seismic recordings yield coherent signals between seismometers [*Shapiro and Campillo*, 2004]. Thus, under certain conditions, coherent seismic signal can be generated "at will" from ambient noise. Based on this principle, coherent signals have been reconstructed from noise recordings in such diverse fields as helioseismology [*Rickett and Claerbout*, 2000], ultrasound [*Weaver and Lobkis*, 2001], regional [*Shapiro and Campillo*, 2004; *Sabra et al.*, 2005; *Bensen et al.*, 2007] and exploration [*Draganov et al.*, 2007] seismology, and for ocean acoustic waves [*Roux and Kuperman*, 2004]. In this article, we exploit the existence of the ambient infrasonic fluctuations known as microbaroms [*Bowman et al.*, 2005; *Tanimoto and Artru-Lambin*, 2007] to show the same methods are applicable to atmospheric infrasound. Microbaroms are closely related to microseisms, which have been widely used in ambient noise seismology [*Shapiro and Campillo*, 2004], and represent the interaction of the ocean with the atmosphere instead of the solid Earth. Although microbaroms often determine the background noise level on infrasound recordings worldwide [*Bowman et al.*, 2005], we demonstrate that their long-range correlation properties allow them to be used as signal. From analysis of continuous recordings using two infrasound microphones at Fourpeaked Volcano, Alaska, we are able to measure the infrasonic impulse response and relate its variation to temperatures in the atmospheric boundary layer. These observations motivate the monitoring of atmospheric structure with ambient infrasound noise.

2. Data

[4] We select 18 days of continuous data from co-located infrasound microphones and short-period seismometers at two sites (station codes FONW and FOSS) on Fourpeaked Volcano, Alaska, shown in Figure 1 (left). The volcano was first instrumented in 2006 in response to volcanic activity beginning on September 17, 2006 [*Cervelli and West*, 2007]. The 18 days of continuous recordings we use in this study are taken from late February and early March 2007 and cover UTC days 52 through 70 during 2007. Although small explosions occurred intermittently, signals of volcanic origin (e.g., tremor) did not dominate the continuous recordings during this time period. In addition to infrasonic and seismic data at Fourpeaked Volcano, we analyze temperature records from ocean buoys in the Shelikof Strait (buoy 46077), on Augustine Island (buoy AUGA2), and at the mouth of the Cook Inlet (buoy AMAA2). Wind data is analyzed from the buoy on Augustine Island.

[5] Sites FONW and FOSS are telemetered in real-time to the Alaska Volcano Observatory for the purpose of monitoring. The sites are located at elevations of 905 and 1268 m for FONW and FOSS, respectively; Fourpeaked Volcano reaches a peak elevation of 2104 m. The seismometers are vertical component L4 Mark Products short-period instruments with a corner frequency at 1 Hz. The

[1] Alaska Volcano Observatory, U.S. Geological Survey Alaska Science Center, Anchorage, Alaska, USA.
[2] Now at Department of Geosciences, Boise State University, Boise, Idaho, USA.

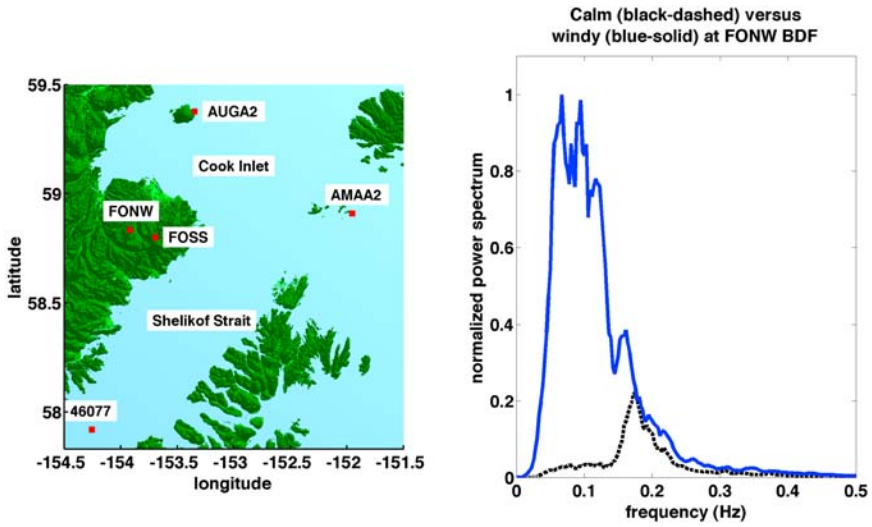

Figure 1. (left) Regional map of Fourpeaked volcano, located at the southern end of the Cook Inlet, Alaska. Co-located infrasonic microphones and seismometers exist at two sites, FONW and FOSS, within the local monitoring network. Three nearby buoys measure temperature (46077, AMAA2, and AUGA2) and wind data (AUGA2). (right) A comparison of the power spectrum between 0 and 0.5 Hz at station FONW for an hour from a windy day (day 56) and a calm day (day 62); note the microbarom peak at 0.2 Hz.

infrasound data is collected by Chaparral Model 2 microphones on the high-gain channel. Both the infrasound and seismic data are recorded at a sample rate of 100 Hz. The system response of the infrasonic microphones is flat between 0.1 and 50 Hz [*Petersen et al.*, 2006].

3. Methods

[6] We extract coherent signals between FONW and FOSS from ambient noise by applying the same correlation-based methodology to both the seismic and infrasound data. We use the processing sequence originally developed for continuous seismic data [*Bensen et al.*, 2007] and work with non-overlapping hour-long segments. Prior to cross-correlation, we decimate and time-normalize the signal and then whiten the spectrum over the frequency band of interest, from 0.2 to 0.5 Hz. Decimation reduces the original sampling rate from 100 Hz to 10 Hz, which is more than sufficient for analyzing signals below 1 Hz. For time normalization, we employ a running RMS filter that applies a weight to each sample that is inversely proportional to the RMS amplitude within a 10 s window around the sample. The time-normalization acts to reduce the impact of non-stationary parts of the time series such as earthquakes and noise spikes. Spectral whitening is achieved by dividing the complex spectrum by a smoothed version of the amplitude spectrum. The decimated, time-normalized, and whitened signals for both the infrasound and seismic data are cross-correlated with each other and the resulting correlation is saved for each hour-long time interval. Correlations averaged over longer time intervals are calculated by simply summing the individual hour-long cross-correlations. In this study, we find that applying a 10-hour-long moving average to the successive hour-long correlations offers a reasonable tradeoff between convergence of the impulse response and time resolution. Thus, each correlation attributed to a particular time is in fact the average of the correlations spanning 5 hours before and after that time.

4. Observations

[7] The dominant characteristics of the infrasound impulse responses can be deduced through comparisons with meteorological and seismic data. In Figure 2a, the most recognizable feature from the ambient infrasound noise correlations for FONW and FOSS is a coherent arrival with variable amplitude at time lags between −40 and −45 s. With FONW and FOSS separated by 13.5 km, these time lags agree well with speeds (300−340 m/s) expected for a direct infrasound wave in the atmosphere. The arrival only appears for the negative time-lags, corresponding to a wave propagating westward from FOSS to FONW, instead of eastward from FONW to FOSS as expected for positive lags. Such an asymmetry for noise correlations (arrivals at either positive or negative time-lags) is often observed for seismic data [*Shapiro and Campillo*, 2004; *Bensen et al.*, 2007] and is indicative of the direction to the microseismic source region. Propagation from FOSS to FONW supports a source region for the microbaroms to the east of FOSS. Note that the arrival times of the seismic correlations are significantly more stable than their infrasound counterparts, pointing to atmospheric path effects for the infrasound. Coherent seismic arrivals register over the 18 days at time-lags of approximately −5 s. This delay time corresponds to a wave speed of 2.7 km/s, a reasonable value of fundamental mode Rayleigh wave velocity for frequencies from 0.2 to 0.5 Hz in Alaska. The seismic noise correlations are similarly limited to negative time-lags, suggesting that their source region is in the same eastern direction as the infrasound noise correlations.

[8] A striking example of the dependence of the infrasound noise correlation on atmospheric conditions is evident from a comparison with temperature and wind data

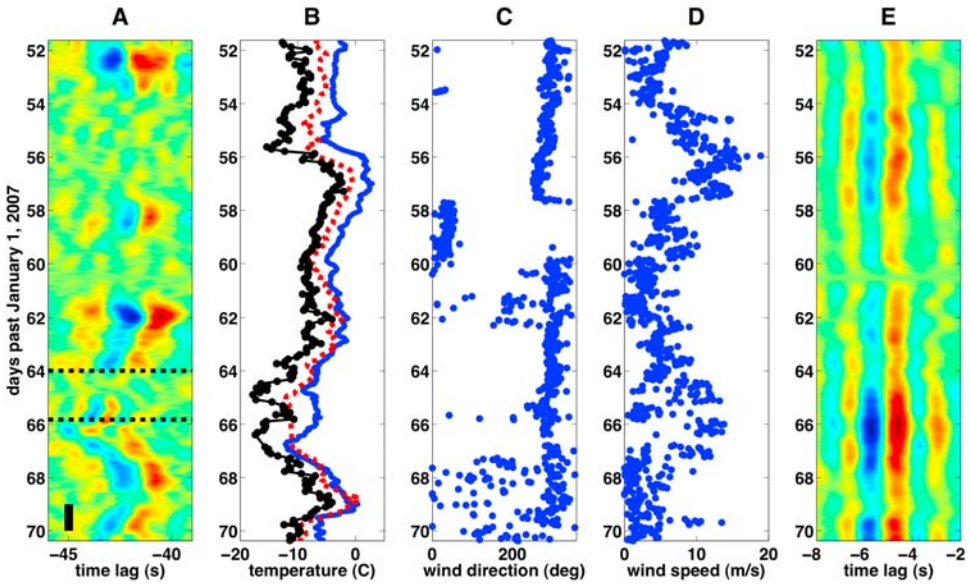

Figure 2. (a) Comparison over 18 days of the infrasound noise correlation between stations FONW and FOSS, (b) temperature data at buoys 46077 (blue line), AUGA2 (black dotted-line), and AMAA2 (red dashed-line), (c) wind direction (clockwise from north) at buoy AUGA2, (d) wind speed at buoy AUGA2, and (e) the seismic noise correlation between stations FONW and FOSS. The arrival time of the pulse in Figure 2a and the regional temperatures in Figure 2b follow each other closely. The horizontal black dashed lines in Figure 2a denote the time of two repeating explosions shown in Figure 3a. The vertical black line in Figure 2a indicates the time period over which group velocity curves are inverted for time-dependent profiles in Figure 3c and 3d.

measured on nearby ocean buoys. Temperature and wind data for the 18 days are plotted in Figures 2b, 2c, and 2d. When the direct wave exists in the infrasound noise correlation, its arrival time closely follows the variation in temperature measured by three regional buoys, as it should since the speed of sound c is directly proportional to the square-root of temperature T, $c \sim \sqrt{T}$. Note in particular the close correspondence between Figure 2a and 2b during day 66 of 2007, at a time of strong temperature variations. The infrasound noise correlation can therefore be used as an acoustic thermometer for the local conditions at Fourpeaked Volcano. From Figure 2c, the winds at AUGA2 are typically from the WNW (300° clockwise from north). Since we have already established that the direct wave propagates from FOSS to FONW, this means that the noise correlation is able to reconstruct the direct wave in the upwind direction. Additional evidence for variations in sound speed comes from two repeating explosions at Fourpeaked Volcano that occurred at the times marked by the horizontal black lines in Figure 2a, on days 64 and 66 of 2007 (2353 UTC March 4 and 1954 UTC March 6). Bandpassed seismic and acoustic recordings (2–4 Hz) at station FOSS for these two explosions are plotted in Figure 3a with alignment based on the seismic signals. The acoustic signal for the later explosion is time-shifted by 0.2 s as a result of reduced sound speed during this time period. The time shift is in agreement with the trend of the noise correlations in Figure 2a. Understanding the time delay between seismic and acoustic signals is important since it can be used to infer properties of the volcanic source [*Petersen et al.*, 2006].

[9] We further explore the characteristics of the direct arrival in the infrasound noise correlation by studying its frequency dependence. Since the amplitude of the infrasound noise correlation varies strongly with time, we focus on the 24 successive noise correlations on March 10, 2007 (day 69 of 2007), at a time when the amplitude displayed stability (see vertical black line in Figure 2a). Application of the multiple-filter technique [*Bensen et al.*, 2007] to the one of the correlations reveals that the group velocity of the infrasound wave is dispersive over the frequency range from 0.2 to 0.5 Hz, as shown in Figure 3b. Dispersion with higher group velocities at lower frequencies supports the existence of a low-level atmospheric waveguide between FOSS and FONW. Infrasonic guided waves in the lower atmosphere have been observed following man-made explosions [*Negraru and Herrin*, 2009]. Guided waves are often observed in the ambient seismic field due to microseisms [*Shapiro and Campillo*, 2004] and have large amplitudes since they experience only 2D geometrical spreading. Group velocity dispersion curves extracted for all 24 correlations on day 69, shown in Figure 3c, have similar dispersion properties superimposed on an overall trend toward lower velocities over the 24 hour period.

5. Group Velocity Inversion for Time-Dependent Sound Speed Profiles

[10] The group velocity dispersion curves in Figure 3c can be explained by a model of an acoustic waveguide created by a time-varying temperature inversion. Under normal conditions, temperature (and thus sound speed) is expected to decrease as a function of height according to the adiabatic lapse rate (−6.5° C/km), prohibiting the formation of a low-velocity waveguide near the surface. However, temperature inversions can occur when dense, cold air sits near the surface as in the case of snow and glacier-covered

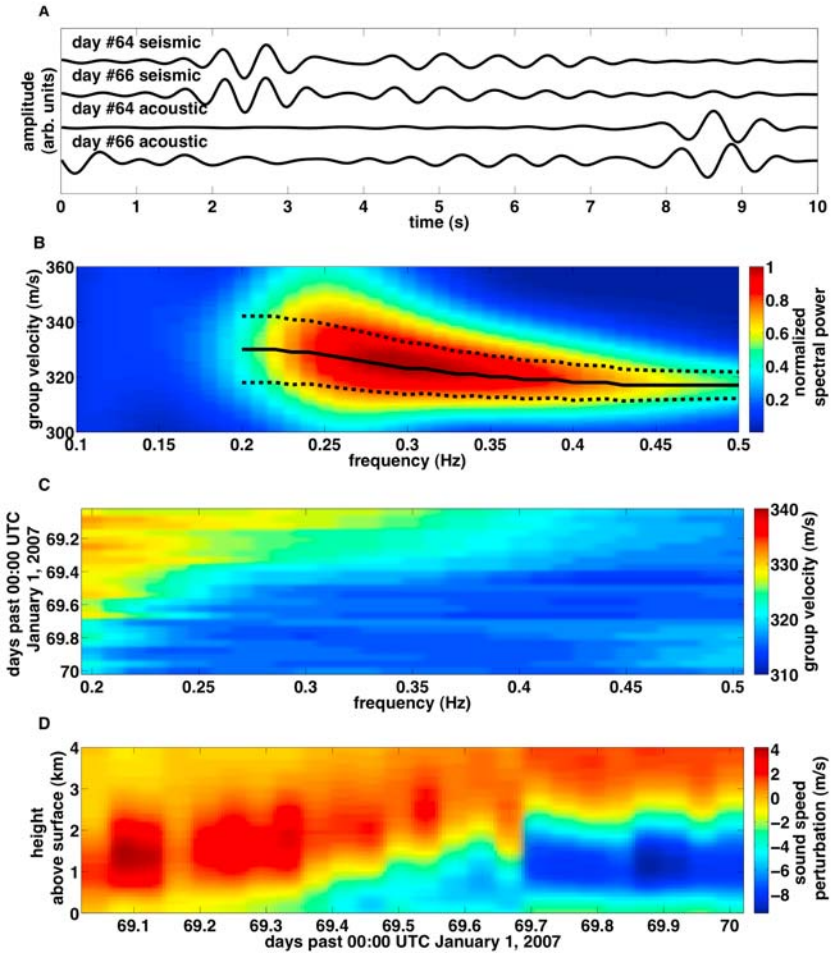

Figure 3. (a) Comparison of two repeating volcanic explosions at station FOSS which occurred at the times shown in Figure 2a. (b) Energy diagram for a single noise correlation from day 69. Error bars are given by a 1 dB reduction from peak power. (c) Group velocities for all of day 69, computed from energy diagrams. (d) Result of inverting the dispersion curves in Figure 3c for an average time-dependent sound speed profile over the 24-hour period.

terrain or during the passage of a weather front [*Whiteman*, 2000]. We explore this possibility by inverting the observed time-dependent group velocity dispersion curves in Figure 3c for average sound speed profiles between FOSS and FONW.

[11] From *Ostashev et al.* [2005], the acoustic pressure field P in a stratified atmosphere without wind effects is given by:

$$\frac{d^2P}{dz^2} - \frac{1}{\rho}\frac{d\rho}{dz}\frac{dP}{dz} + \left(\frac{\omega^2}{c^2} - k^2\right)P = 0, \tag{1}$$

where z is the height above the surface, k is the horizontal wavenumber, ω is the angular frequency, and c is the sound speed. Application of the finite-element method to equation (1), as described by *Lysmer* [1970], leads to an eigenvalue problem for the sampled pressure field $\vec{p}$ as a function of height:

$$\omega^2 A\vec{p} = \left(k^2 B_2 + B_0\right)\vec{p}, \tag{2}$$

where A, B_2, and B_0 are banded matrices dependent on bulk modulus κ and density ρ. At constant frequency, a first order perturbation of wavenumber and material properties in equation (2) gives the relation:

$$\frac{\delta v}{v} = \frac{1}{2k^2\vec{p}^T B_2\vec{p}}\left(\sum_{i=1}^{N}\vec{p}^T\frac{\partial(k^2B_2+B_0)}{\partial\rho_i}\vec{p}\delta\rho_i - \omega^2\sum_{i=1}^{N}\vec{p}^T\frac{\partial A}{\partial\kappa_i}\vec{p}\delta\kappa_i\right) = \vec{j}_v^T\frac{\vec{\delta c}}{c}, \tag{3}$$

where N is the number of finite-elements, $\delta v/v$ is the relative perturbation in phase velocity of the guided infrasound wave at frequency ω, $\vec{j}_v^T$ is a single row of the full Jacobian matrix J_v for phase velocity data, and $\vec{\delta c}/c$ is the vector of relative perturbations of sound speed as a function of height above the surface (the model vector). We use the power law relation $\rho \sim c^{-2.5}$, empirically derived from a year of data at buoy 46077, to relate perturbations in κ and ρ to perturbations solely in terms of c. Using equation (3), phase velocities measured at many frequencies lead to a matrix relation between model and data $\vec{\delta v}/v = J_v\,\vec{\delta c}/c$. As shown by *Rodi et al.* [1975], the Jacobian matrix for group velocity

U, given by $\delta\vec{U}/U = J_U\ \vec{\delta c}/c$, can be calculated in a straightforward manner from the phase velocity Jacobian matrix J_v.

[12] Shown in Figure 3d are the inverted sound speed profiles over the 24 hour period. The profiles are shown in terms of perturbations from an initial model consisting of a simple surface-based sound speed inversion that begins at 310 m/s at the surface and varies smoothly to 330 m/s at a height of 2 km. On average, the linearized inversions for each of the 24 group velocity curves reduced the RMS error by 70% from the initial model. The inverted sound speed profiles in Figure 3d show that the time-dependent, surface-based inversion layer became stronger over the 24 hour period, with a colder, denser, and lower sound speed layer of air moving between FOSS and FONW. This layer, imaged in the lower 2 km of the atmosphere, may represent a strong regional inversion due to the passage of a weather front, a local inversion enhanced by radiative cooling over snow and glacier-covered terrain, or flow blocking of a cold air mass [*Whiteman*, 2000] on the windward (WNW) side of Fourpeaked Volcano. The existence of time-dependent temperature inversions offers an explanation for the variable amplitudes of the infrasound correlations in Figure 2a. Strong infrasound correlations occur during times of temperature inversions, when infrasound energy is guided close to the surface. The theory described above can be applied to individual time periods during other temperature inversions, but it cannot be applied to the 18 days continuously, since periods of temperature inversion are interrupted by periods of normal temperature gradient. In conclusion, these observations open up new approaches for imaging and monitoring the structure of the Earth's atmosphere, in particular the atmospheric boundary layer.

[13] **Acknowledgments.** This work is funded by the USGS Mendenhall postdoctoral program. Temperature and wind data are from the National Data Buoy Center. Thanks to Steve McNutt and Peter Cervelli for reviews.

References

Bedard, A. J., Jr., and T. M. Georges (2000), Atmospheric infrasound, *Phys. Today*, *53*, 32–37.

Bensen, G. D., M. H. Ritzwoller, M. P. Barmin, A. L. Levshin, F. Lin, M. P. Moschetti, N. M. Shapiro, and Y. Yang (2007), Processing seismic ambient noise data to obtain reliable broad-band surface wave dispersion measurements, *Geophys. J. Int.*, *169*, 1239–1260.

Bowman, J. R., G. E. Baker, and M. Bahavar (2005), Ambient infrasound noise, *Geophys. Res. Lett.*, *32*, L09803, doi:10.1029/2005GL022486.

Cervelli, P., and M. West (2007), The 2006 eruption of Fourpeaked Volcano, Katmai National Park, Alaska, *Eos Trans. AGU*, *88*(52), Fall Meet. Suppl., Abstract V31E-0719.

Draganov, D., K. Wapenaar, W. Mulder, J. Singer, and A. Verdel (2007), Retrieval of reflections from seismic background-noise measurements, *Geophys. Res. Lett.*, *34*, L04305, doi:10.1029/2006GL028735.

Lysmer, J. (1970), Lumped mass method for Rayleigh waves, *Bull. Seismol. Soc. Am.*, *60*, 89–104.

Negraru, P., and E. T. Herrin (2009), On infrasound waveguides and dispersion, *Seismol. Res. Lett.*, *80*, 565–571.

Ostashev, V. E., D. K. Wilson, L. Liu, D. F. Aldridge, N. P. Symons, and D. Marlin (2005), Equations for finite-difference, time-domain simulation of sound propagation in moving inhomogeneous media and numerical implementation, *J. Acoust. Soc. Am.*, *117*, 503–517.

Petersen, T., J. Caplan-Auerbach, and S. R. McNutt (2006), Sustained long-period seismicity at Shishaldin Volcano, *J. Volcanol. Geotherm. Res.*, *151*, 365–381.

Rickett, J. E., and J. F. Claerbout (2000), Calculation of the Sun's impulse response by multi-dimensional factorization, *Sol. Phys.*, *192*, 203–210.

Rodi, W. L., P. Glover, T. M. C. Li, and S. S. Alexander (1975), A fast, accurate method for computing group-velocity partial derivatives for Rayleigh and Love modes, *Bull. Seismol. Soc. Am.*, *65*, 1105–1114.

Roux, P., and W. A. Kuperman (2004), Extracting coherent wavefronts from acoustic ambient noise in the ocean, *J. Acoust. Soc. Am.*, *116*, 1995–2003.

Sabra, K. G., P. Gerstoft, P. Roux, W. A. Kuperman, and M. C. Fehler (2005), Extracting time-domain Green's function estimates from ambient seismic noise, *Geophys. Res. Lett.*, *32*, L03310, doi:10.1029/2004GL021862.

Shapiro, N. M., and M. Campillo (2004), Emergence of broadband Rayleigh waves from correlations of the ambient seismic noise, *Geophys. Res. Lett.*, *31*, L07614, doi:10.1029/2004GL019491.

Tanimoto, T., and J. Artru-Lambin (2007), Interaction of solid earth, atmosphere and ionosphere, in *Treatise in Geophysics*, vol. 4, edited by G. Schubert, pp. 421–444, Elsevier, Oxford, U. K.

Weaver, R. L., and O. I. Lobkis (2001), Ultrasonics without a source: Thermal fluctuation correlations at MHz frequencies, *Phys. Rev. Lett.*, *87*, 134301, doi:10.1103/PhysRevLett.87.134301.

Whiteman, C. D. (2000), *Mountain Meteorology*, Oxford Univ. Press, New York.

Wilson, D. K., and D. W. Thomson (1994), Acoustic tomographic monitoring of the atmospheric surface layer, *J. Atmos. Oceanic Technol.*, *11*, 751–769.

M. M. Haney, Department of Geosciences, Boise State University, Boise, ID 83725, USA. (matt@cgiss.boisestate.edu)